Biosensors and Bioelectronics 23 (2008) 1825–1831

Contents lists available at ScienceDirect

Biosensors and Bioelectronics

journal homepage: www.elsevier.com/locate/bios

Electrochemically fabricated polypyrrole nanofiber-modified electrode as a new electrochemical DNA biosensor

Kh. Ghanbari [a], S.Z. Bathaie [b], M.F. Mousavi [b,*]

[a] Department of Chemistry, Tarbiat Modares University, Tehran, Iran
[b] Department of Clinical Biochemistry, Faculty of Medical Sciences, Tarbiat Modares University, Tehran, Iran

ARTICLE INFO

Article history:
Received 18 November 2007
Received in revised form 24 February 2008
Accepted 25 February 2008
Available online 18 March 2008

Keywords:
Electrochemical DNA biosensor
Polypyrrole nanofiber
Spermidine
Pulse voltammetry
EIS

ABSTRACT

A new biosensor employing immobilized DNA on a nano-structured conductive polymer fixed onto a platinum electrode is presented. Upon optimization of synthesis parameters, polypyrrole nanofibers, 30–90 nm in diameter, were synthesized in an aqueous media by the electropolymerization of pyrrole using normal pulse voltammetry (NPV). The nanofiber film was investigated by scanning electron microscopy (SEM), cyclic voltammetry (CV) and electrochemical impedance spectroscopy (EIS). Double-stranded DNA was physisorbed onto the PPy nanofiber films. Various parameters, including the pH and DNA concentration, were optimized. The DNA immobilized on the nanofiber films was characterized using differential pulse voltammetry (DPV) and Fourier-transform infrared (FTIR) spectroscopy. Using DPV to study the interaction of spermidine with DNA, a binding constant (K) value of $4.08 \times 10^5 \pm 0.05\,M^{-1}$ was obtained. For the determination of spermidine, the proposed method exhibited a good dynamic range, correlation coefficient (0.05–1.0 μM and 0.9983, respectively) and a low detection limit (0.02 μM), although Ca^{2+} ions were found to electrostatically bind to DNA and weaken the spermidine–DNA interaction.

1. Introduction

Nanotechnology is rapidly evolving to discover new materials useful in solving challenging bioanalytical problems, including specificity, stability and sensitivity (Ramanavičius et al., 2006). The unique properties of nanoscale materials offer excellent prospects for interfacing biological recognition events with electronic signal transduction in order to design a new generation of bioelectronic devices with novel functions.

Conducting polymers are very effective substrates for biomaterial immobilization. Some conducting polymers are doped and/or covalently or physically modified by bionanomaterials, especially proteins and nucleic acids, which exhibit unique catalytic (Malinauskas, 1999) or affinity (Ramanavičienė and Ramanavičius, 2004) properties that can be easily employed in the design of biosensors. Among other conducting polymers, polyaniline is often used as an immobilizing substrate for biomolecules (Geise et al., 1991) and as an efficient electrocatalyst (Yuan et al., 2007). However, to detect bio-analytes at a physiological pH, biosensing materials must be electroactive in neutral environments, unlike polyaniline and polythiophene. To overcome this problem, PPy is very attractive because it is more easily deposited from neutral pH aqueous solutions of pyrrole monomers (Ramanavičius et al., 2006).

The normal pulse voltammetry (NPV) method for synthesis of nanofibers (Ghanbari et al., 2006; Bard and Stratmann, 2003) has many advantages. The sharp concentration gradient of the pulse allows for a higher mass transport than a hydrodynamic electrode, giving more visible kinetic effects.

Since the first report on the electrochemical behavior of nucleic acids by Paleček, many studies in this area have been performed (Paleček, 1996; Paleček and Fojta, 2001). Double-stranded DNA (dsDNA) immobilized on the surface of an electrode can be used as the recognition element of affinity biosensors to detect small molecules (drugs, carcinogens, pollutants) that interact with DNA (Rodriguez et al., 2005; Wang et al., 2002).

The intracellular concentrations of SPD (NH_2–$(CH_2)_4$–NH–$(CH_2)_3$–NH_2) or spermine are critical for determining whether a cell proceeds through its cycle or undergoes apoptosis (Ha et al., 1997). High levels of polyamines have also been associated with many diseases such as cancer, infections, insulin-dependent diabetes mellitus and Alzheimer's disease (Gambaro et al., 2004).

Since they are positively charged at physiological pH, polyamines are thought to act by electrostatic binding to macromolecules, such as nucleic acids, to stabilize them and/or possibly facilitate their conformational shifts (Feurstein et al., 1990). Direct interactions between polyamines and nucleic acids were proposed

* Corresponding author at: P.O. Box 14115-175, Tehran, Iran. Tel.: +98 21 82883474; fax: +98 21 88006544.
E-mail addresses: mousavim@modares.ac.ir, mfmousavi@yahoo.com (M.F. Mousavi).

0956-5663/$ – see front matter © 2008 Elsevier B.V. All rights reserved.
doi:10.1016/j.bios.2008.02.029

based on different techniques including precipitation, thermal denaturation and FTIR (Cohen, 1998; Ruiz-Chica et al., 2001). The efficiency of polyamines and polyamine analogues in protecting dsDNA from oxidative breakage and radiation has been suggested (Ha et al., 1998a,b).

Various methods have been described for the determination of polyamines (Gambaro et al., 2004; Li et al., 2006; Zhang et al., 2005). Since most amines show neither natural UV absorption nor fluorescence, most methods require that amines be separated and derivatized before direct or indirect detection (Kovács et al., 1999). However, chemical modifications are unpredictable and protracted, result in dilution of the sample, which affects the process, and are difficult to apply to very small sample volumes. To avoid unwieldy pre- and post-column derivatizations, reversed phase or cation-exchange chromatography separation followed by electrochemical detection has also been studied; however, such techniques consume large amounts of reagents, including organic solvents. Thus, there is great interest in developing a method for the determination of polyamines in biological samples, especially foods, that is simple, rapid and reliable (Sun et al., 2003). Based on our survey, no reports of an electrochemical method for the determination of SPD and SPD–DNA interactions exist in the literature.

Following our recent studies (Heli et al., 2004, 2005; Ghanbari et al., 2006), we herein report the use of NPV for the synthesis of PPy nanofibers on a platinum electrode. The effects of various parameters on the electroactivity of these films are also investigated. DNA physisorbed onto PPy is characterized using DPV and FTIR. As a new electrochemical biosensor, this electrode is applied to study the interaction of SPD with DNA/PPy nanofiber films.

2. Experimental

2.1. Materials

Double-stranded calf thymus DNA was purchased from Fluka and suspended in Tris–EDTA buffer (10 mM Tris base, 1 mM EDTA solution, pH 8). Prior to use, pyrrole (Aldrich) was distilled under vacuum. All other reagents including SPD, HCl, NaOH, $LiClO_4$, Na_2HPO_4 and NaH_2PO_4 were of analytical grade from Fluka or Merck. The concentration of DNA was calculated according to the absorbance at 260 nm using $\varepsilon_{DNA} = 0.02\ ml\ \mu g^{-1}$ (Wang et al., 1999). All solutions were prepared using double-distilled, deionized water.

2.2. Instrumentation

All electrochemical measurements were carried out in a conventional three electrode cell, powered by an Autolab PGSTAT 30 galvanostat/potentiostat (Eco Chemie, The Netherlands) connected to a computer, an Ag/AgCl reference electrode, a platinum (Pt) disk working electrode (Metrohm, 2 mm diameter) and a Pt plate counter electrode. Micrographs were obtained using a Philips model X-30 scanning electron microscope (SEM). FTIR spectra were obtained on a MB102 spectrometer (Bomem, Quebec, Canada).

2.3. Electrochemical synthesis and characterization of polypyrrole nanofibers

Electropolymerization of polypyrrole nanofibers, performed by NPV, involved the immersion of a Pt disk electrode into a solution of pyrrole containing a synthesis buffer of 0.1 M $LiClO_4$ and 0.2 M phosphate buffer solution (PBS). A series of potential pulses was imposed from 0.0 to 0.80 V (versus Ag/AgCl). The amount of increase in the potential increment (PI) at each new step and between successive pulses was kept constant. In the next cycle, the electrode potential returned to 0.0 V and the process was repeated twice. For comparison, a PPy film was also prepared using the CV method by repeatedly cycling the potential from 0.0 to 0.80 V (versus Ag/AgCl) for 100 cycles at a sweep rate of 50 mV s^{-1}. Each Pt electrode coated with PPy film was then washed with distilled water and dried.

Prepared PPy-coated electrodes were analyzed by CV and EIS. Measurements were performed in an analysis buffer consisting of 0.05 M PBS and 0.1 M $LiClO_4$, with a pH of 7.4. The frequency range extended from 10 kHz to 40 mHz, with an ac potential perturbation of 5 mV r.m.s. The impedance data were analyzed and fitted by Zplot/Zview software (Scribner Associates Inc.).

2.4. Immobilization of dsDNA

Prior to immobilization, the PPy nanofiber-coated electrode was transferred to a 10 mM NaCl + 10 mM Tris–HCl buffer (pH = 3.0) for electrochemical oxidation of the PPy layer at 0.5 V (versus Ag/AgCl) for 5 min. After that, different amounts of DNA (0.5–5 μl of a 4 mg/ml stock solution) were physisorbed onto the nanofiber films on the Pt electrode. Prior to use, these DNA/PPy films were dried overnight in a desiccator and then washed with 5 ml PBS (0.05 M, pH 7.4) to remove unadsorbed DNA. These DNA/PPy films were stored desiccated at 25 °C until use.

2.5. Optimization and characterization of the DNA/PPy nanofiber films

The effects of the amount of DNA (2–20 μg) and pH (4–8) of the PBS (0.05 M) on the DNA/PPy films were evaluated according to the variation of the peak current of the differential pulse voltammograms obtained for the DNA/PPy films. These DNA/PPy films were further characterized by FTIR. The DNA/PPy films were then transferred to a SPD solution for voltammetric measurement (DPV). These experiments were carried out in an analysis buffer consisting of PBS and $LiClO_4$ (0.05 M/0.1 M, pH 7.4). The DPV conditions used were as follows: step potential, 10 mV; pulse amplitude, 50 mV; scan rate, 10 mV s^{-1}.

3. Results and discussion

3.1. Electrochemical investigations of PPy films

Two PPy films were synthesized, one using CV and the other using NPV, and their electroactivities were studied using CV and EIS (Fig. 1).

As shown in the cyclic voltammograms for the PPy films prepared by CV and NPV in Fig. 1A (curve a and b, respectively), the anodic peak current density at ca. 0.36 V, attributed to the doping process of the PPy film, was characteristic of the electroactivity of the PPy film. As the redox processes of PPy were carried out through the doping–undoping of anions in the PPy films, the doping–undoping resistances of the anions are directly represented in the redox peak currents. Although both methods used the same experimental conditions, the PPy film formed using NPV (Fig. 1A curve b) has a higher redox-switching rate, which is represented by a significantly higher anodic peak current than that of the PPy film formed by CV (Fig. 1A curve a). Thus, the PPy films prepared by different electrochemical methods have different electroactivities.

The impedance spectra of the conducting polymer are used to evaluate film conductivity, film structure and charge transport at the polymer film/electrolyte interface. Nyquist diagrams and Bode plots for the PPy films prepared by NPV and CV at the open circuit potential (OCP) are shown in Fig. 1B and C, respectively. As seen in Fig. 1B, the electrochemical behavior of the modified electrode

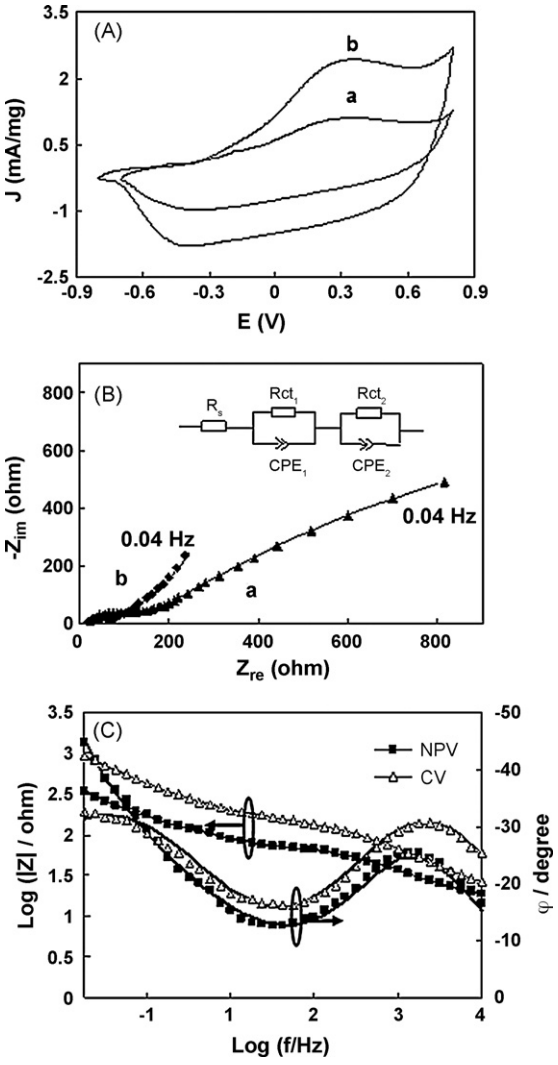

Fig. 1. Cyclic voltammograms (A), Nyquist diagrams (B) and Bode plots (C) of PPy films synthesized by (a) CV and (b) NPV (C_{py} = 0.1 M, PI = 4 mV, PD = 0.4 s), in 0.05 M PBS and 0.1 M $LiClO_4$, at pH 7.4. Scan rate for CVs: 50 mV s^{-1}. In the Nyquist diagrams, points are experimental data and solid lines are fitted curves. Inset B: equivalent circuit for PPy film.

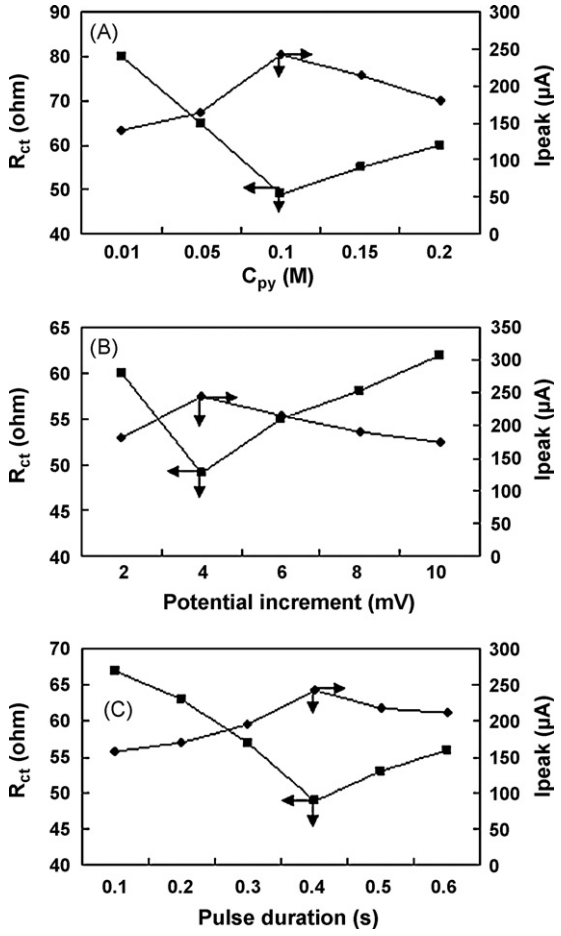

Fig. 2. Influence of synthesis parameters on the PPy film R_{ct} (■) using EIS at the OCP, and I_p (♦) using CV. (A) C_{py}: 0.01–0.2 M (PI = 4 mV, PD = 0.4 s). (B) PI: 2–10 mV (C_{py} = 0.1 M, PD = 0.4 s). (C) PD: 0.1–0.6 s (C_{py} = 0.1 M, PI = 4 mV). PPy films were prepared by NPV method in 0.05 M PBS and 0.1 M $LiClO_4$ solution, at pH 7.4; scan rate for CVs: 50 mV s^{-1}.

has two charge-transfer steps. The first semicircle represents the ionic charge-transfer resistance at the electrolyte–polymer interface (R_{ct1}). The second semicircle is attributed to the R_{ct} at the polymer–electrode interface (R_{ct2}). Additionally, Fig. 1C is a typical representation of the corresponding Bode plot. Here, both Bode plots clearly show the two-step process during the electrochemical studies and confirm the Nyquist plot findings.

According to the impedance spectra of the polymer films coated on Pt disk electrodes, in the asymmetric metal/film/electrolyte configuration, an equivalent circuit, shown in the inset of Fig. 1B, represents the impedance behavior of the PPy films prepared by CV and NPV at the OCP. In this circuit, R_s represents the electrolyte solution resistance. The two observed charge-transfer semicircles correspond to two RC parallel combinations, and are due to the ionic R_{ct1} in parallel to the first constant phase element (CPE_1) and the R_{ct2} in parallel to the CPE_2. Electron transfer occurs at the polymer–electrode interface, while, at the polymer–electrolyte interface, we expect an anion transfer for charge compensation. The PPy film prepared by NPV (Fig. 1B curve b) has a lower R_{ct1} (44.8 Ω) than the PPy film prepared by CV (Fig. 1B curve a, 149.2 Ω) and, consequently, exhibits a higher doping/undoping rate and conductivity. In all cases, fit errors were lower than 10%. There is good agreement between the EIS and CV results, considering the proportional decrease in R_{ct1} for the NPV-synthesized PPy polymer (Fig. 1B) compared to that of the CV-synthesized polymer, as displayed by the increase in the current density in the voltammograms (Fig. 1A).

3.2. Influence of synthesis parameters on the electroactivity of PPy films prepared by NPV

Fig. 2A illustrates the changes in the anodic peak current (I_p) and R_{ct} measured by CV and EIS, respectively, for the product formed with NPV at pyrrole concentrations ranging from 0.01 to 0.2 M at a PI of 4 mV and a pulse duration (PD) of 0.4 s. As the monomer concentration (C_{py}) increases from 0.01 to 0.1 M, the I_p increases and the R_{ct} decreases. However, at C_{py} values over 0.1 M, the anodic I_p decreases and the R_{ct} increases.

Fig. 2B shows the effect of the PI on the R_{ct} and I_p of the PPy film, as measured by EIS and CV, respectively. We examined the product formed using NPV at PIs ranging from 2 to 10 mV (C_{py} = 0.1 M, PD = 0.4 s). The I_p increases with PI, with a maximum value at 4 mV. The I_p decreases as the PI increases beyond 4 mV. The least R_{ct} is also observed at a PI of 4 mV.

Fig. 2C shows the effect of PD on the R_{ct} and I_p in the spectra and voltammograms of the PPy films prepared by NPV. We exam-

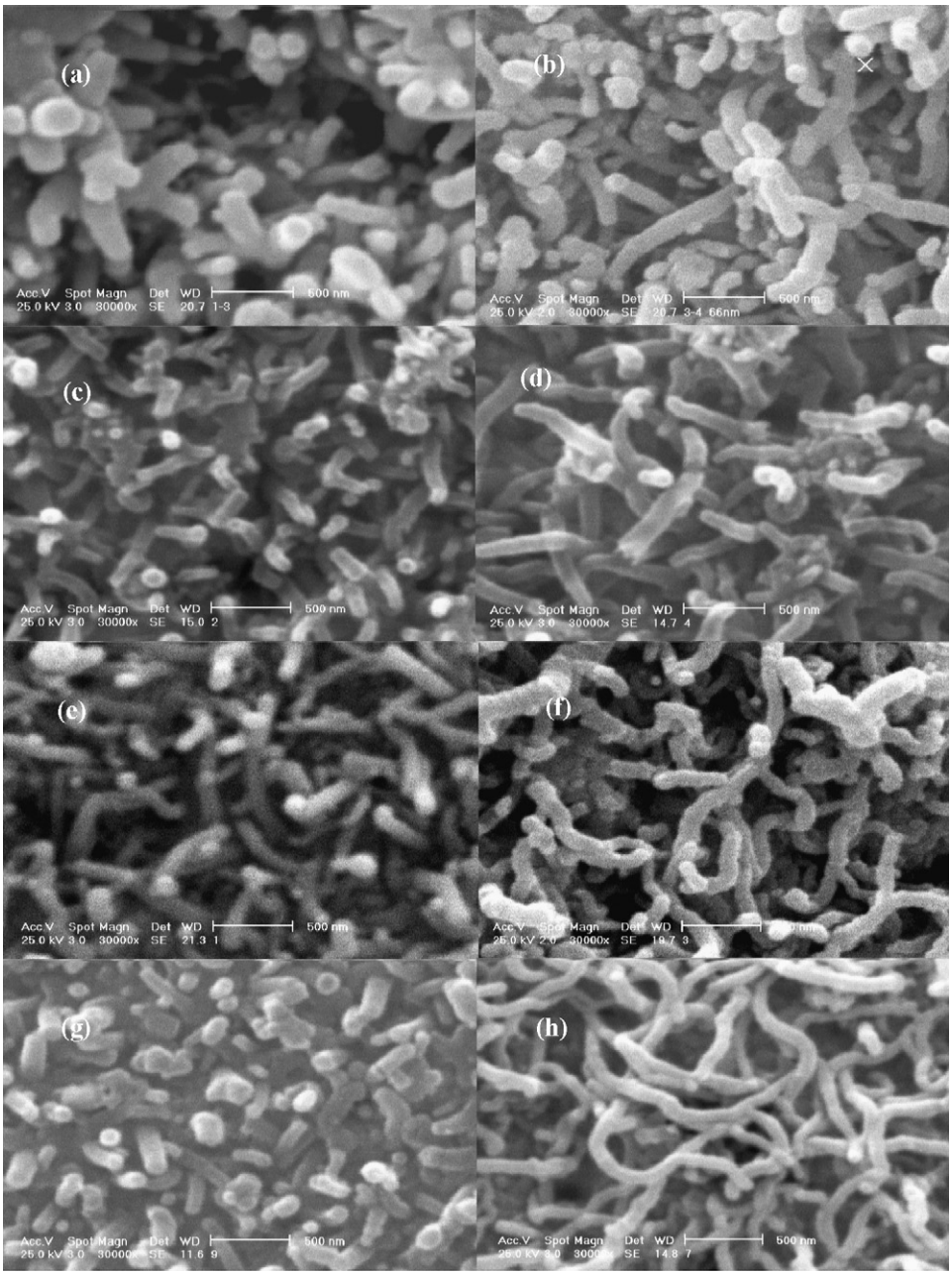

Fig. 3. SEM images comparing the PPy films prepared by (a) CV and (b) NPV (C_{py} = 0.1 M, PD = 0.1 s, PI = 6 mV). Synthesis conditions of NPV-prepared PPy films: C_{py} (c) 0.02 M; (d) 0.15 M (PD = 0.4 s, PI = 4 mV); PI (e) 2 mV; (f) 10 mV (C_{py} = 0.1 M, PD = 0.4 s); PD (g) 0.2 s, (h) 0.4 s (C_{py} = 0.1 M, PI = 4 mV).

ined the film formed using NPV pulses ranging from 0.1 to 0.6 s in duration (C_{py} = 0.1 M, PI = 4 mV). As seen in Fig. 2C, the R_{ct} decreases with an increase in PD, so that the least R_{ct} is observed at a PD of 0.4 s. However, the I_p increases with PD, and the maximum value appears at 0.4 s, beyond which there is a decrease in I_p.

3.3. *Influence of synthesis conditions on the morphology of PPy films prepared by CV and NPV*

In order to evaluate the two types of synthesis, we compared the polymer morphology of the films synthesized by the CV (Fig. 3a) and NPV methods (Fig. 3b). The SEM images reveal that stocky, rod-like structures were created using CV and much finer filamentous structures by NPV. Therefore, the NPV method was used to synthesize films in the optimization of synthesis parameters.

The morphological differences induced at various C_{py}s (0.05–0.2 M) were investigated. SEM images reveal that the nanofiber morphology created at a pyrrole concentration of 0.05 M (Fig. 3c) is much finer than that formed at 0.15 M (Fig. 3d).

Typical SEM images of the nanofibers in the PPy film formed at a potential of 2 mV (Fig. 3e) is only slightly finer than that at 10 mV (Fig. 3f).

Increasing the PD in the range of 0.1–0.6 s shows dramatic differences in the morphology of PPy nanofibers. As shown in the SEM images, a pulse of 0.2 s results in short, thick fibers with diameters of 150–200 nm (Fig. 3g) and a 0.4 s pulse produces much longer, thinner fibers, approximately 30–90 nm by 5 μm (Fig. 3h). As the PD increases, the duration of the imposed potential at each pulse is longer. According to the polymerization mechanism proposed by Sadki et al. (2000), the formation

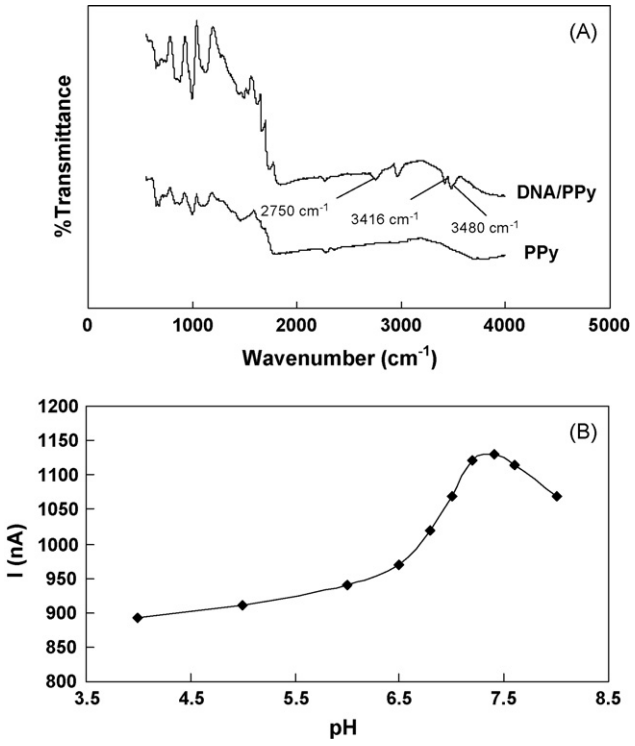

Fig. 4. (A) FTIR spectrum of the PPy nanofiber films with and without adsorbed DNA. (B). Influence of pH on the guanine oxidation signals at the DNA/PPy nanofiber electrode, in a solution of 0.05 M PBS with 0.1 M $LiClO_4$.

of oligomers with more pyrrole units produces much longer fibers.

Therefore, as we would expect, given the same size electrode, the PPy film with the finest nanofibers (Fig. 3h) has a larger actual surface area to accommodate the electrochemical reaction than that of the film made of the thicker PPy fibers synthesized by the CV method. Consequently, the NPV-synthesized film has a lower doping–undoping R_{ct1}, and shows a faster anionic doping–undoping rate and a higher I_p in the corresponding CVs (Fig. 1A). These results help to explain why NPV-nanofiber PPy films have a higher electroactivity. For NPV polymerization, the potential varies periodically. During the anodic potential, the pyrrole monomer is polymerized and converted to the PPy fiber at the electrode/solution interface. Then, during the cathodic potential, polymerization ceases and PPy changes from the oxidized state to the reduced state. The consumed pyrrole monomer is supplemented during the cathodic period; therefore, the PD also influences the polymerization of the pyrrole. According to electrochemical crystallography theory, when the potential varies from cathodic to anodic, PPy nuclei are formed on the electrode surface. The size and density of these nuclei are related to the difference between cathodic and anodic potential. As polarization proceeds, PPy nuclei continuously grow together, eventually becoming PPy films. In this way, the PD affects the growth process of PPy and, hence, PPy morphology.

3.4. Optimization of DNA immobilization

3.4.1. FTIR investigation of DNA/PPY nanofiber film

Fig. 4A shows the FTIR spectra of the PPy-nanofiber films in the presence and absence of DNA. The characteristic vibrational peaks for PPy are observed at 2945 cm^{-1} (aromatic C–H), 1687 cm^{-1} (C=N), 1350 cm^{-1} (C–N), 1176 cm^{-1} (phenyl ring C=N), 1120 and 1070 cm^{-1} (O=N), and 825 cm^{-1} (phenyl ring C–H). The 1614 cm^{-1} vibration band is due to the C=C bond associated with C–N stretching and bending vibration. Similar peaks have been reported previously (Gambhir et al., 2001).

There are some changes in the FTIR peaks of the PPy film after interaction with DNA, including those at 3480 and 3416 cm^{-1}, associated with the NH stretching vibration of nucleic acid bases, and at 2750 cm^{-1}, associated with the NH–N hydrogen bonds. There are also peaks for guanine, cytosine, adenine and thymine at 1720, 1496, 1610, and 1670 cm^{-1}, respectively. The slight shifts in these peaks compared to those reported by Prabhakar et al. (2007) may be attributed to the interaction of DNA with the PPy nanofiber.

3.4.2. Effect of DNA concentration

The immobilization of different amounts of DNA, from 2 to 20 μg, onto the PPY nanofiber film was investigated. The guanine oxidation peak current was used as an indicator to obtain the maximum surface coverage of the film as determined by DPV (Petrovykh et al., 2003). As shown in Fig. 5A curve a, guanine was oxidized at approximately +0.85 V. The oxidation current increases with an increase in the amount of DNA adsorbed onto the DNA/PPY nanofiber film. This can be ascribed to the increased number of guanine molecules available for oxidation. It has been reported that guanine-rich regions of DNA serve as multiple hops resulting in an increased oxidation current due to enhanced charge mobility in nearby GC (guanine–cytosine) base pairs (Troisi and Orlandi, 2001).

It appears that the guanine oxidation current decreases in the presence of more than 10 μg DNA (Jiang and Wang, 2001) and becomes constant above 15 μg DNA (data not shown).

3.4.3. Effect of pH

The pH effect on guanine oxidation at the DNA/PPy nanofiber film was carried out at room temperature, in a pH range of 4.0–8.0, and measured using DPV (Fig. 4B). The guanine oxidation current increases with the increase in pH from 4.0 to 7.4, after which a decrease in the oxidation current is observed. This result might be assigned to the over-oxidation of the PPy nanofiber film or to the decreased electrical conductivity of the PPy nanofiber films at pH >7.4 (Uang and Chou, 2003).

3.5. DNA–SPD interaction

As shown in Fig. 5A, the DPVs of the DNA/PPy electrode nicely exhibit the oxidation of guanine in the absence (a) and presence of 1.0 μM SPD (b). The addition of SPD causes a considerable diminution in the guanine oxidation peak current (curve b) as the binding of SPD to the DNA guanine bases shields the oxidizable groups of guanine and inhibits its oxidation.

The binding of the SPD to dsDNA is dependent on the interaction time. The guanine peak current decreased as the time increased up to 4 min, after which the decrease in the guanine peak current leveled off and remained constant up to 6 min (data not shown). Therefore, in all of the subsequent experiments, a 5-min interaction time was used.

Fig. 5B shows the effect of the SPD concentration (0.02–1.0 μM) on DPV signals. A linear dependence of the guanine peak currents was observed in the range of 0.05–1.0 μM ($r = 0.9983$), with a detection limit of 0.02 μM.

The value of the binding constant for the interaction of SPD with DNA is determined using Eq. (2) as described by Ibrahim (2001), for immobilized ligand on an electrode. For our purposes, the equation was modified slightly according to the nature of the immobilized molecule by replacing ligand with DNA, as follows:

$$\text{DNA} + \text{spermidine} \rightleftharpoons \text{DNA–spermidine} \quad (1)$$

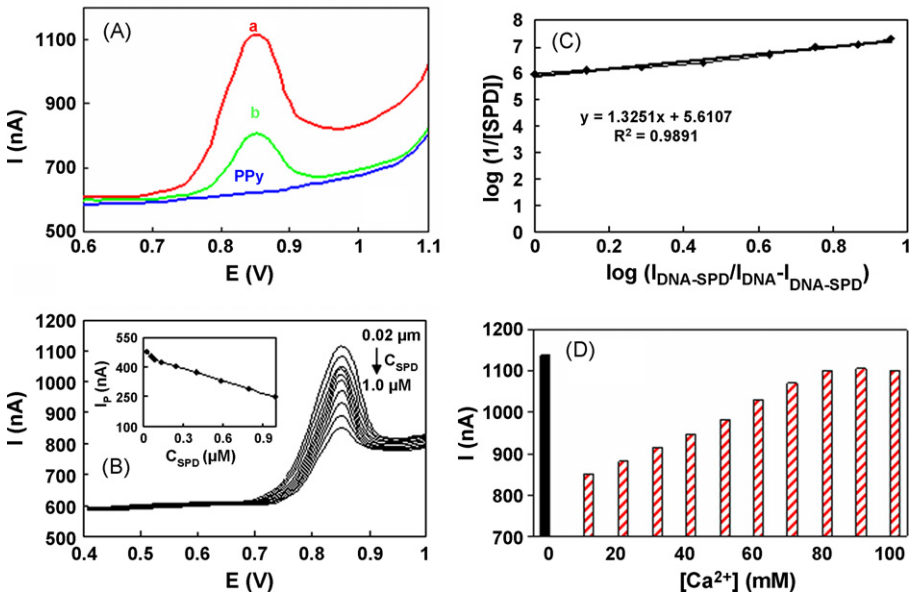

Fig. 5. (A) DPVs of the PPy film and guanine oxidation signals at the DNA/PPy nanofiber electrode in absence (a) and presence (b) of SPD (1.0 μM). (B) DPVs at various concentrations of SPD (0.02–1.0 μM). Inset: calibration curve of I_p versus C_{SPD}. (C) Determination of K for the interaction of SPD with DNA, in 0.05 M PBS and 0.1 M $LiClO_4$, at pH 7.4: log(1/[SPD]) versus log($S_{DNA-SPD}/S_{DNA} - S_{DNA-SPD}$). (D) Effect of Ca^{2+} on the SPD–DNA interaction of the electrochemical DNA biosensor (hatched column). The black column shows Ca^{2+} with the DNA biosensor in the absence of SPD.

$$\log\left(\frac{1}{[\mathrm{SPD}]}\right) = \log K + \log\left(\frac{S_{\mathrm{DNA-SPD}}}{S_{\mathrm{DNA}} - S_{\mathrm{DNA-SPD}}}\right) \quad (2)$$

where K is the apparent binding constant, S_{DNA} is the signal in the case of immobilized DNA alone, and $S_{DNA-SPD}$ is the signal of the DNA–SPD complex on the electrode. S is the peak current obtained using DPV. As shown in Fig. 5C, the value of K can be determined from the intercept of the straight line, obtained from the corresponding DPV. The value of the binding constant determined by this technique is $4.08 \times 10^5 \pm 0.05\ M^{-1}$ (%RSD = 0.7%). This value is consistent with the previously reported constant of $1.4 \times 10^5\ M^{-1}$, obtained using affinity capillary electrophoresis (Ouameur and Tajmir-Riahi, 2004).

SPD has at least two different modes of binding to dsDNA: (i) a nonspecific, electrostatic interaction, which involves binding between the protonated amino groups of SPD and the negatively-charged phosphate groups of DNA, and (ii) minor groove binding (Ohishi et al., 2008; Ruiz-Chica et al., 2001). The affinity of DNA for cations is reported to have the following order: $Ca^{2+} > Mg^{2+} \gg Na^+ \cong K^+$ (Korolev et al., 1999). Ca^{2+} interacts with the phosphate groups of DNA and the N(7) nitrogens of guanine, forming chelated complexes (Kornilova et al., 1995). Thus, to determine the effect of Ca^{2+} on the interaction of SPD with DNA, we titrated a solution containing a fixed concentration of SPD (1.0 μM) with increasing concentrations of $CaCl_2$ from 10 to 100 μM (Fig. 5D). The addition of Ca^{2+} enhanced the SPD-induced decrease in the guanine oxidation peak current, as measured by DPV. This indicates that SPD attaches to the negatively-charged surface of the phosphate backbone of DNA, an interaction which overcomes the minor groove binding. As the Ca^{2+} concentration increases, SPD molecules start to bind to the minor groove, due to the establishment of the ionic shielding of the negative charges on DNA. At approximately 80 μM Ca^{2+}, the guanine oxidation peak current reached a constant value, approximating the value seen in the absence of SPD. This signifies the removal of SPD from the DNA layer in the presence of Ca^{2+}. Similar behavior has been observed for ciprofloxacin in the presence of Ca^{2+} (Nawaz et al., 2006).

Table 1
Comparison of the analytical performance for determination of SPD by DNA/PPy electrode with classical methods

Technique used	Linear range (μM)	LOD[a] (μM)	r[b]	Reference
DPV	0.05–1.0	0.02	0.9983	This work
CZE[c]	0.05–3.0	0.03	0.9996	Zhang et al. (2005)
CE[d]	2–200	0.01	0.9967	Sun et al. (2003)
IC-IPAD[e]	0.7–34.4	0.4	0.9999	Borba and Rohrer (2007)

[a] Limit of detection.
[b] Correlation coefficient.
[c] Capillary zone electrophoresis.
[d] Capillary electrophoresis.
[e] Ion chromatography with integrated pulsed amperometric detection.

In our investigation of the interaction of SPD with DNA immobilized on the CV-synthesized PPy film, we found a linear decrease in the guanine oxidation peak current from 1.0 to 15.0 μM ($r = 0.991$), with a detection limit of 0.8 μM. The value of the binding constant determined using DPV was $4.0 \times 10^5 \pm 0.03\ M^{-1}$ (%RSD = 0.5%). These results, compared with those obtained under the same conditions using the NPV-fabricated PPy nanofiber film, show that the latter has a higher specific area, with a larger capacity to physisorb more DNA, resulting in a wide linear range and a more sensitive detection limit for the interaction of DNA with SPD. These results were also compared with those obtained by other researchers, as shown in Table 1.

To examine the effects of interfering ligands (I), we calculated the ratio of i_{SPD+I}/i_{SPD}, where i_{SPD} = response current to 0.5 μM SPD and i_{SPD+I} = response current to 0.5 μM SPD in presence of 0.5 μM of I. Where I was spermine or the neutrally-charged minor groove binders, crocin or crocetin (Bathaie et al., 2007). The i_{SPD+I}/i_{SPD} ratios obtained were 0.89, 1 and 1, respectively, indicating that the electrode is specific for positively-charged polyamines.

We studied the variation of the guanine oxidation peak current for the DNA/PPy electrodes, to determine the effectivity of electrode performance over time. The DNA/PPy electrodes were found

to have a shelf-life of about 30 days when stored under desiccated conditions at 25 °C (data not shown).

4. Conclusions

PPy nano-structured films prepared by the NPV method were found to possess good electroactivity due to their high specific surface area. Synthetic parameters have a great influence on the electrochemical properties of the PPy film. The film with the best electroactivity is obtained using the NPV method under the following conditions: PI = 4 mV, PD = 0.4 s and C_{py} = 0.1 M. We have further shown that when DNA is physisorbed onto this PPy nanofiber film-coated Pt electrode, the resulting electrochemical biosensor detects DNA–SPD interaction using the oxidation of guanine in the DNA. The main advantages of this sensor are the rapid detection, low cost, wide dynamic range, good correlation coefficient and low detection limit, as well as its effectiveness at physiological pH.

Acknowledgement

The support of the Tarbiat Modares University Research Council is gratefully acknowledged.

References

Electroanalytical Chemistry. Bard, A.J., Stratmann, M. (Eds.), 2003. Encyclopedia of Electrochemistry, vol. 3. Wiley, pp. 112–113.
Bathaie, S.Z., Bolhasani, A., Hoshyar, A., Ranjbar, B., Sabouni, F., Moosavi-Movahedi, A.-A., 2007. DNA Cell Biol. 26, 533–540.
Borba, B.M.D., Rohrer, J.S., 2007. J. Chromatogr. A 1155, 22–30.
Cohen, S.S., 1998. A Guide to the Polyamines. Oxford University, New York.
Feurstein, B.G., Pattabiraman, N., Marton, L.J., 1990. Nucleic Acids Res. 18, 1271–1282.
Gambaro, V., Casagni, E., Dell'Acqua, L., Valenti, M., Visconti, G.L., 2004. J. Pharm. Biomed. Anal. 35, 409–413.
Gambhir, A., Gerared, M., Hain, S.K., Malhotra, B.D., 2001. Appl. Biochem. Biotechnol. 96, 303–309.
Geise, J.R., Adams, J.M., Barone, N.J., Yacynych, A.M., 1991. Biosens. Bioelectron. 6, 151–160.
Ghanbari, Kh., Mousavi, M.F., Shamsipur, M., 2006. Electrochim. Acta 52, 1514–1522.
Ha, H.C., Woster, P.M., Yager, J.D., Casero Jr., R.A., 1997. Proc. Natl. Acad. Sci. U.S.A. 94, 11557–11562.
Ha, H.C., Sirisoma, N.S., Kuppusamy, P., Zweier, J.L., Woster, P.M., Casero Jr., R.A., 1998a. Proc. Natl. Acad. Sci. U.S.A. 95, 11140–11145.
Ha, H.C., Yager, J.D., Woster, P.A., Casero Jr., R.A., 1998b. Biochem. Biophys. Res. Commun. 244, 298–303.
Heli, H., Bathaie, S.Z., Mousavi, M.F., 2004. Electrochem. Commun. 6, 1114–1118.
Heli, H., Bathaie, S.Z., Mousavi, M.F., 2005. Electrochim. Acta 51, 1108–1116.
Ibrahim, M.S., 2001. Anal. Chim. Acta 443, 63–72.
Jiang, M., Wang, J., 2001. J. Electroanal. Chem. 500, 584–589.
Kornilova, S.V., Kapinos, L.E., Blagoi, I., 1995. Mol. Biol. (Moscow) 29, 574–584.
Korolev, N., Lyubartsev, A.P., Rupprecht, A., Nordenskiod, L., 1999. Biophys. J. 77, 2736–2749.
Kovács, Á., Simon-Sarkadi, L., Ganzler, K., 1999. J. Chromatogr. A 836, 305–313.
Li, J.S., Wang, H., Huang, K.J., Zhang, H.S., 2006. Anal. Chim. Acta 575, 255–261.
Malinauskas, A., 1999. Synth. Met. 107, 75–83.
Nawaz, H., Rauf, S., Akhtar, K., Khalid, A.M., 2006. Anal. Biochem. 354, 28–34.
Ohishi, H., Odoko, M., Grzeskowiak, K., Hiyama, Y., Tsukamoto, K., Maezaki, N., Ishida, T., Tanaka, T., Okabe, N., Fukuyama, K., Zhou, D., Nakatani, K., 2008. Biochem. Biophys. Res. Commun. 366, 275–280.
Ouameur, A.A., Tajmir-Riahi, H.A., 2004. J. Biol. Chem. 279, 42041–42054.
Paleček, E., 1996. Electroanalysis 8, 7–14.
Paleček, E., Fojta, M., 2001. Anal. Chem. 75, 83A.
Petrovykh, D.Y., Kimura-Suda, H., Whitman, L.J., Tarlov, M.J., 2003. J. Am. Chem. Soc. 125, 5219–5226.
Prabhakar, N., Arora, K., Singh, S.P., Pandey, M.K., Singh, H., Malhotra, B.D., 2007. Anal. Chim. Acta 589, 6–13.
Ramanavičienė, A., Ramanavičius, A., 2004. In: Thomas, D.W. (Ed.), Advanced Biomaterials for Medical Applications. Kluwer Academic Publishers, Netherlands.
Ramanavičius, A., Ramanavičienė, A., Malinauskas, A., 2006. Electrochim. Acta 51, 6025–6037.
Rodriguez, M.C., Kawde, A.N., Wang, J., 2005. Chem. Commun. 34, 4267–4269.
Ruiz-Chica, J., Medina, M.A., Sánchez-Jiménez, F., Ramirez, F.J., 2001. Biophys. J. 80, 443–454.
Sadki, S., Schottland, P., Brodie, N., Sabouraud, G., 2000. Chem. Soc. Rev. 29, 283–293.
Sun, X., Yang, X., Wang, E., 2003. J. Chromatogr. A 1005, 189–195.
Troisi, A., Orlandi, G., 2001. Chem. Phys. Lett. 344, 509–518.
Uang, Y.M., Chou, T.C., 2003. Biosens. Bioelectron. 19, 141–147.
Wang, Y.T., Zhao, F.L., Li, K.A., Tong, S.Y., 1999. Anal. Chim. Acta 396, 75–81.
Wang, G., Xu, J.J., Chen, H.Y., 2002. Electrochem. Commun. 4, 506–509.
Yuan, J., Han, D., Zhang, Y., Shen, Y., Wang, Z., Zhang, Q., Niu, L., 2007. J. Electroanal. Chem. 599, 127–135.
Zhang, L.Y., Tang, X.C., Sun, M.X., 2005. J. Chromatogr. B 820, 211–219.